H2S gas sensing mechanism of SnO2 films with ultrathin CuO dotted islands

doi: 10.1063/1.1490154

H_2S gas sensing mechanism of SnO_2 films with ultrathin CuO dotted islands

Arijit Chowdhuri,[a] Parmanand Sharma, Vinay Gupta, and K. Sreenivas
Department of Physics and Astrophysics, University of Delhi, Delhi-110007, India

K. V. Rao
Department of Material Science, TmFy-Royal Institute of Technology (KTH), Stockholm SE-10044, Sweden

(Received 14 January 2002; accepted for publication 8 May 2002)

H_2S gas interaction mechanisms of sputtered SnO_2 and SnO_2-CuO bilayer sensors with a varying distribution of the Cu catalyst on SnO_2 are studied using Pt interdigital electrodes within the sensing film. Sensitivity to H_2S gas is investigated in the range 20–1200 ppm. Changes induced on the surface, the SnO_2-CuO interface, and the internal bulk region of the sensing SnO_2 film upon exposure to H_2S have been analyzed to explain the increasing sensitivity of three different sensors SnO_2, SnO_2-CuO, and SnO_2 with CuO islands. SnO_2 film covered with 0.6 mm diameter ultrathin ($\sim$10 nm) CuO dots is found to exhibit a high sensitivity of 7.3×10^3 at a low operating temperature of 150 °C. A response speed of 14 s for 20 ppm of H_2S, and a fast recovery time of 118 s in flowing air have been measured. The presence of ultrathin CuO dotted islands allow effective removal of adsorbed oxygen from the uncovered SnO_2 surface due to spillover of hydrogen dissociated from the H_2S-CuO interaction, and the spillover mechanism is sensed through the observed fast response characteristics, and the high sensitivity of the SnO_2-CuO-dot sensor. © *2002 American Institute of Physics.* [DOI: 10.1063/1.1490154]

I. INTRODUCTION

H_2S detection is of great importance in many fields such as commercial gas and oil exploration, autoventilation units, and the medical field of dentistry.[1,2] The threshold for human tolerance is reported to be 20 ppb, and as such there is a continued interest for designing new sensing materials and heterolayer structures with improved sensitivity.[3] Semiconducting tin oxide (SnO_2) with suitable metal additives shows better selectivity and sensitivity to various reducing gases.[1,4] Maekawa *et al.*[4] found that the sensitivity increases with decreasing electronegativity of doped cations in SnO_2. Surprisingly, the Cu^{2+} cation exhibited a high sensitivity ($S=35\,000$ for 50 ppm H_2S at 200 °C), and sintered pastes loaded with CuO showed a fast recovery, but the response was slow.[4] In the last decade sintered pastes,[5] thick,[6] and thin film structures[7,8] using mixed SnO_2-CuO powders, $Cu-SnO_2$ bilayers,[7] and $CuO-SnO_2$ heterocontacts,[8] have been extensively investigated, and their performances are compared in Table I. Wide variations in the reported test conditions and the response characteristics are noted. Instances where a high sensitivity is observed, the response time is often found to be slow (3–175 min), and a fast response time (15–180 s) is noticed mostly for higher H_2S concentration.[9,10] Processing conditions significantly influence the response characteristics. For example, $CuO-SnO_2$ sputtered bilayers[7,8] subjected to different heat treatment exhibited different sensing characteristics (Table I). Recently, chemical fixation of CuO onto spin coated SnO_2 films from sol solutions exhibited a high sensitivity and lowered the detection limit down to a few ppm, but the response speed was slow (in min).[11,12]

The high sensitivity of CuO doped SnO_2 sensors has been attributed primarily to the electronic interaction between the *p*-type CuO and the *n*-type polycrystalline SnO_2 grains[13] and the effect of H_2S gas in reducing the barrier height.[14] In mixed oxide structures the slow response speed has been identified with the statistical distribution of *p-n* junctions throughout the bulk, and the limited penetration of H_2S molecules to the interior regions of the bulk.[12]

Ultrathin bilayer structures are found more suitable for achieving a fast response because the shorter diffusion paths of the interacting gas molecule can be effectively utilized. Vasiliev *et al.*,[8] prepared a planar CuO/SnO_2 thin film heterostructure by sputtering and contacted the layers separately with Au electrodes. The top CuO layer was found insensitive to H_2S and yielded a low sensitivity ($S=70$ at 17 ppm) and a slow response (in min). In contrast, Jianping *et al.*,[7] measured the resistance of SnO_2 with underlying platinum electrodes, and reported a critical CuO over layer thickness of 7 nm for achieving a maximum sensitivity ($S=80$ at 1 ppm), but the response speed was slow.[7] More recently Gadkari *et al.*[15] reported a degradation mechanism explaining decrease in sensitivity associated with over and under usage of evaporated $CuO-SnO_2$ bilayers.

Morrison[16] proposed two mechanisms of catalyst control on gas sensors: (a) Fermi level energy control mechanism and (b) spillover mechanism. In the Fermi-level energy control mechanism, the sensing gas converts CuO to CuS and varies the barrier height at the intergranular boundaries after exchanging electrons. In the spillover mechanism the metal-

[a]Author to whom correspondence should be addressed; electronic mail: arijitc123@rediffmail.com

TABLE I. Comparison of reported data on H_2S gas sensors.

Sensor material	Process	H_2S gas concentration (ppm)	Sensitivity	Operating temperature (°C)	Response speed	Reference
$CuO-SnO_2$	spray pyrolysis		75	200	3 min	22
$CuO-SnO_2$	coevaporation	10	130	200	10 min	3
$CuO-SnO_2$	calcined paste	50	35 000	250	40 min	4
ZrO_2-SnO_2	sintered powder	10	500	190	50 min	5
$CuO-SnO_2$	sputtered bilayer	16	70	160	50 min	8
$CuO-SnO_2$	spray pyrolysis	100	2500	200	60 min	2
$CuO-SnO_2$	spin coating	0.3	2000		35 min	12
Pd/SnO_2	spray pyrolysis		2000/5000	300	175 min	23
$Ag-SnO_2$	evaporation	200	35	110	15 s	9
$PdO-SnO_2-Fe_2O_3$	PECVD	800	15	225	30 s	10
$Al_2O_3-SnO_2$	screen printing	40	100	300	60 s	6
$CuO-SnO_2$	sputtered bilayer	10	80	200	100 s	7
$Ag-SnO_2$	sputtering	1	20	150	1000 s	24
$CuO-SnO_2$	sputtering	20	7341	150	14 s	Present work

lic catalyst dissociates the gas molecule, and reactive atoms spill over the semiconductor surface and influence its conductivity. However the enhanced response expected from the spillover mechanism has not yet been demonstrated with an appropriate $CuO-SnO_2$ bilayer structure.

In this work the electronic and chemical interactions on SnO_2 with ultrathin CuO dotted islands have been analyzed. Response characteristics are compared with those of a simple SnO_2 sensor and a SnO_2-CuO bilayer. The distribution of CuO on SnO_2 is shown to promote a fast spillover of hydrogen for enhancing the sensitivity and the response speed.

II. EXPERIMENT

Interdigital electrodes as shown in Fig. 1(a) were prepared on a borosilicate glass substrate by sputtering platinum films through a mask. The electrodes were covered with a 120 nm thick SnO_2 layer deposited by a rf diode reactive sputtering technique using a metallic tin target (Cerac Inc., 99.999%) in $Ar+O_2$ ambient. There was no substrate heating during SnO_2 deposition and the film deposition conditions are listed in Table II. In all the structures a 120 nm thick SnO_2 film was deposited under identical conditions. A 10 nm Cu film was deposited uniformly on the SnO_2 surface to obtain a SnO_2-Cu bilayer structure, and Cu was evaporated through a mesh (0.6 mm pore size) to obtain the SnO_2-Cu-dot sensor. We expect the copper layer deposited through the mask to be thinner (<10 nm) due to shadowing effects. After deposition, the SnO_2-Cu bilayer structures were slowly heated in air at 300 °C for 20 min for achieving a stable resistance. The annealing treatment was considered sufficient to transform the ultrathin Cu layer to CuO in agreement with earlier observations.[17] The three different kinds of sensors are shown in Figs. 1(b)–1(d). The interdigital electrodes (IDE) were intentionally located inside the

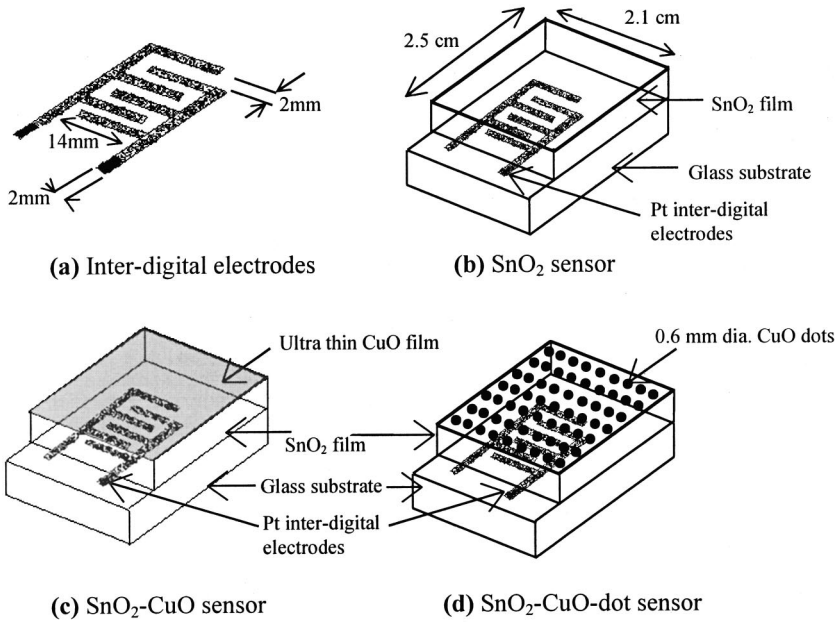

FIG. 1. Construction details of SnO_2, SnO_2-CuO, and SnO_2-CuO-dot sensors with underlying Pt interdigital electrodes.

TABLE II. SnO_2 thin film deposition conditions.

Technique	rf diode sputtering
Target	Tin (99.999%)
Gas	50% Ar+50% O_2
Sputtering pressure	14 mTorr
Power	150 W
Substrate to target distance	7.5 cm
Substrate	borosilicate glass
Substrate temperature	25 °C (no heating)

sensing film (SnO_2) to measure the actual change of resistance of the SnO_2 layer, and offered a high sensitivity in comparison to planar electrodes.

Sensitivity and response speed were measured as a function of temperature (60–250 °C) at different concentration levels of H_2S gas. In view of the corrosive reaction of H_2S gas with metallic surfaces, all contacts inside the test chamber were sputter coated with platinum. The sensor was placed on a temperature controlled heating block, and spring-loaded platinized contacts were used to measure the sensor response. At each temperature the sensor was first stabilized in air to obtain a stable resistance value. H_2S at a specific concentration level was injected into the chamber and response characteristics were recorded using an automatic data acquisition system. Prior to every new measurement the test chamber was purged with atmospheric air for 10 min at the sensor operating temperature to remove previous traces of H_2S gas. The sensitivity factor is defined as

$$S = R_a / R_g \tag{1}$$

where R_a is the resistance of the sensor in atmospheric air, and R_g is the resistance in the presence of reducing gas. The gas concentration characteristics were examined in the range 20–1200 ppm of H_2S at the optimum operating temperature of the sensors where they exhibited a maximum in their sensitivity. The surface morphology of the three sensors before and after exposure to H_2S gas was examined using a Burleigh personal scanning probe microscope (SPM), and images were acquired over an area $2\times2\ \mu m^2$ in the contact mode using a microfabricated Si cantilever (length: 200 μm, width: 40 μm).

III. RESULTS AND DISCUSSION

A. Sensitivity

Figure 2(a) shows the variation in the sensitivity at a constant H_2S gas concentration (20 ppm) as a function of temperature for the three different sensors: SnO_2, SnO_2-CuO, and $SnO_2-CuO-dot$. A maximum in the sensitivity is found to occur at 150 °C for both the SnO_2-CuO bilayer sensors, and for the plain uncovered SnO_2 sensor the maximum occurred at a higher temperature (170 °C). The sensitivity of the SnO_2-CuO-dot sensor ($S\sim7.3\times10^3$) is found to be quite high in comparison to the uncovered SnO_2 ($S\sim11$) and the SnO_2-CuO ($S\sim170$) bilayer sensors. The variation in sensitivity with temperature [Fig. 2(a)] clearly exhibited a maximum at a certain temperature (T_{max}) and thereafter it decreased. The increase in the sensitivity can be attributed to the accelerating rate of irreversible chemisorption reaction due to interaction with the H_2S gas, which tends to reach equilibrium at the critical temperature (T_{max}). Figure 2(b) shows the variation in resistance of all three sensors in air and in the presence of H_2S gas. The resistance R_a in air for all three sensors shows a continuous decrease with increasing temperature. However, beyond the critical temperature (T_{max}), the chemisorption phenomenon slows down and yields a higher value of R_g with increasing temperature [Fig. 2(b)], and therefore the sensitivity ($S=R_a/R_g$) decreases beyond the critical temperature. A sensitivity of $S\sim7.3\times10^3$ for the SnO_2-CuO-dot sensor at 20 ppm of H_2S is found to be high in comparison to some of the high values reported earlier (Table I), and the operating temperature (150 °C) is also found to be low.

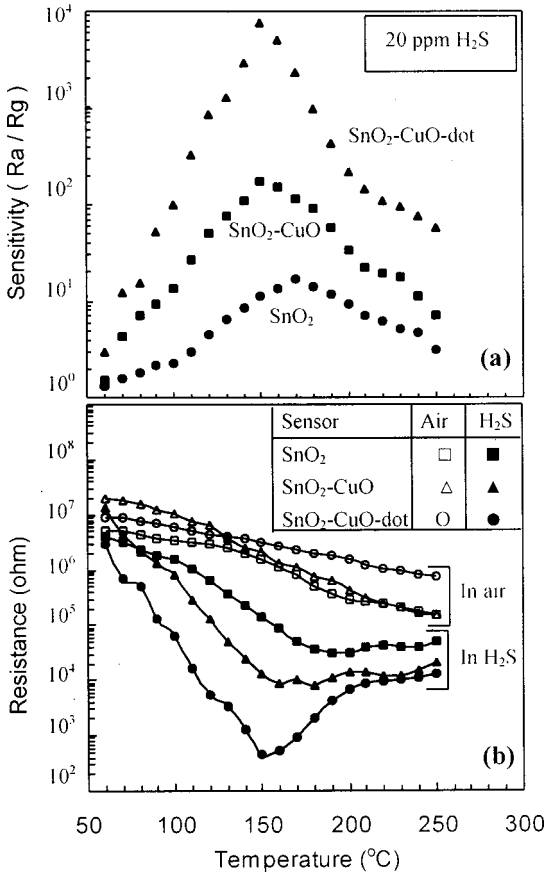

FIG. 2. (a) Temperature dependence of sensitivity of the three sensors, and (b) temperature dependence of sensors resistance (R_a and R_g) before and after exposure to 20 ppm of H_2S.

B. Response characteristics

The sensors were operated at the temperature (T_{max}) where they exhibited a maximum sensitivity. The response transients of the three sensors for 20 ppm H_2S gas are shown in Fig. 3. The SnO_2-CuO-dot sensor exhibited a fast response time of 14 s, whereas the SnO_2-CuO sensor and the uncovered SnO_2 sensor showed a slow response of 33 and 65 s, respectively. The observed response time is found to be quite fast in comparison to earlier reported data (Table I). Liu

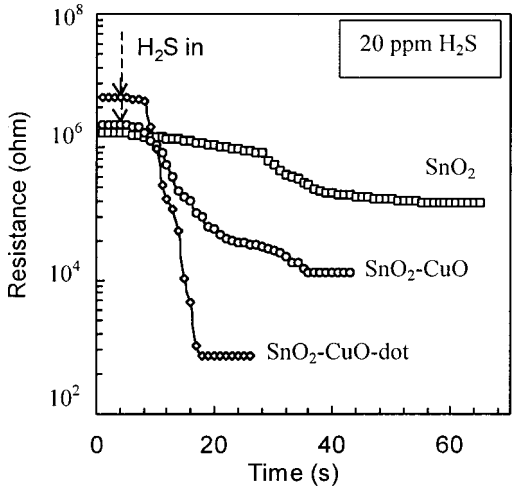

FIG. 3. Response speed of (a) SnO_2, (b) SnO_2-CuO, and (c) SnO_2-CuO-dot sensors at their operating temperature.

et al.[9] observed a similar response speed (15 s) for the SnO_2-Ag bilayer, but the reported sensitivity ($S=35$) at 20 ppm of H_2S was quite low.

Figure 4 shows the response and the recovery characteristics of the three sensors for 20 ppm of H_2S. The recovery was studied both under static (constant air) and dynamic (flowing air) conditions at the optimum operating temperatures. In the static condition the SnO_2-CuO-dot sensor exhibited a fast recovery (481 s) in comparison to the SnO_2-CuO and the SnO_2 sensors which showed a recovery time of 550 and 615 s, respectively. However under the dynamic condition the SnO_2-CuO-dot sensor exhibited a significant improvement with a recovery time of 118 s and its profile is also included in Fig. 4.

The recovery characteristics showed some interesting features marked as phase I and phase II in Fig. 4. The SnO_2 sensor in phase I showed a fast rise whereas the SnO_2-CuO-dot sensor [Fig. 4(c)] exhibited a very slow rise. This is in contrast to the later stage (phase II) where the SnO_2-CuO-dot sensor exhibits a rapid rise in comparison to other two sensors. The fast rise for SnO_2 sensor in phase I is attributed to the quick adsorption of oxygen on its entire surface. However, for the SnO_2-CuO-dot sensor the slow rise in phase I, and a rapid rise in phase II suggested that changes occurring both at the SnO_2-CuO interface and on the surface of uncovered SnO_2 play an important role. The mechanisms relating to the changes that affect the response and recovery in phase II have been discussed in the latter part of the article.

C. Electrical equivalent circuits of the sensors

As the preparation conditions were same for the two SnO_2-CuO structures, it was of interest to understand the sensing mechanisms that influenced the response characteristics of the SnO_2-CuO-dot structure in relation to the other sensor. Specifically the SnO_2-CuO-dot sensor exhibited a fast response, a higher starting resistance prior to H_2S injection (Fig. 3), and a very low resistance in the presence of H_2S, and a high sensitivity. The differences in the construc-

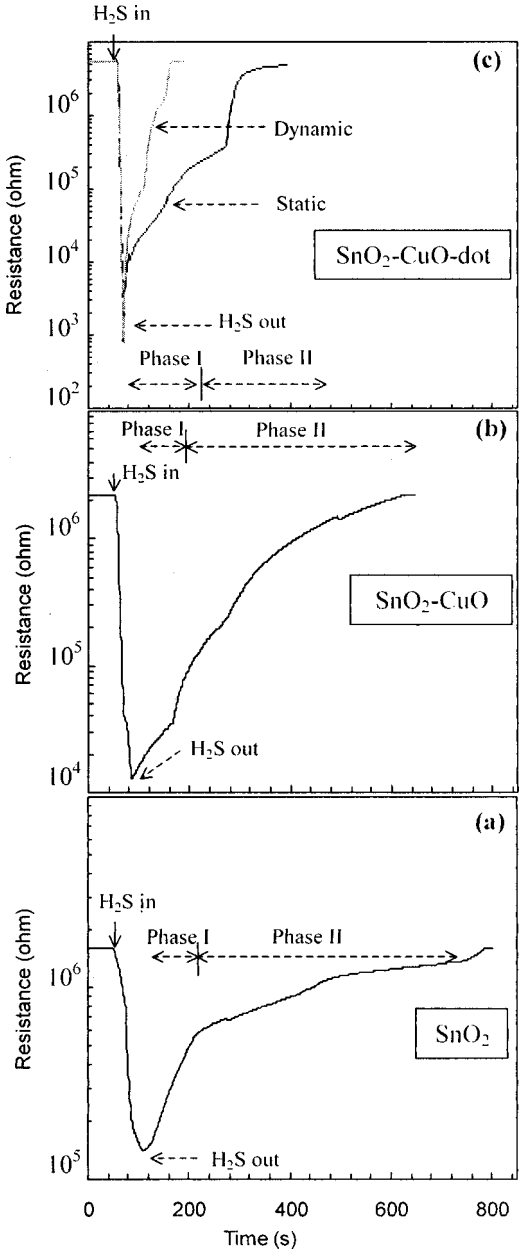

FIG. 4. Response and recovery characteristics of (a) SnO_2, (b) SnO_2-CuO, and (c) SnO_2-CuO-dot sensors for 20 ppm H_2S gas.

tion of the two SnO_2-CuO sensor structures, their electrical equivalents, and the expected changes occurring at the SnO_2-CuO interface are shown schematically in Fig. 5.

The resistance of the SnO_2 layer ($R_1=R_{SnO_2}$) is assumed to be the same in all three sensors because the SnO_2 film thickness and its deposition conditions were kept identical. R_{CuO} is the resistance of the CuO layer deposited on SnO_2 either as a continuous layer, or dispersed in the form of dotted islands (Fig. 5). Resistors R_{SnO_2} and R_{CuO} are in parallel in both the arrangements. R_2 and R_3 represent the equivalent sensor resistance of the SnO_2-CuO, and the SnO_2-CuO-dot structures, respectively [Figs. 5(a) and 5(b)]. It may be noted from Fig. 5 that R_2 and R_3 are not expected to be greater than R_1, because they are individually a parallel combination of R_{SnO_2} (or R_1) and R_{CuO}. At the operating

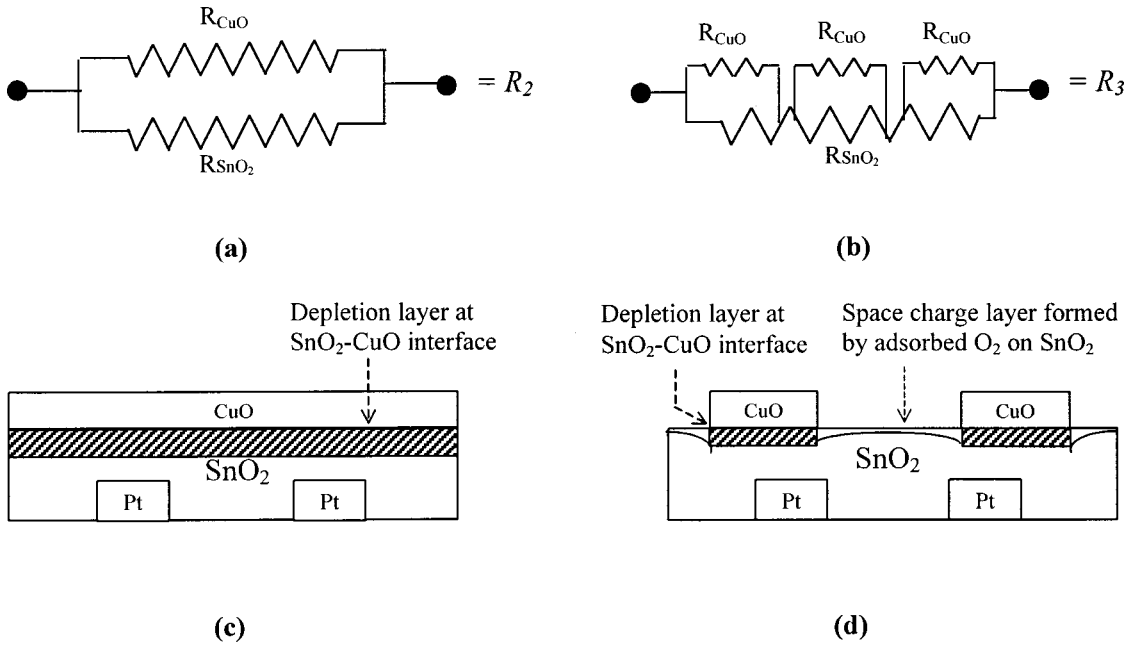

FIG. 5. Electrical equivalent circuits and cross-sectional views of (a) and (c) SnO_2-CuO bilayer, and (b) and (d) SnO_2-CuO-dot sensors.

temperature ($T_{max}=150\,^{\circ}C$), the sensor resistances R_1, R_2, and R_3 of the three sensors are reduced correspondingly to R_1', R_2', and R_3' due to their semiconducting behavior. Similarly R_2' and R_3' ought to be less than R_1' based on the same premise as discussed earlier. However, the measured starting resistance of the three sensors before exposure to H_2S are in the order $R_3'>R_2'>R_1'$ as seen from the response characteristics shown in Fig. 3. In the presence of H_2S gas, R_3', R_2', and R_1' are further decreased to R_3'', R_2'', and R_1'', respectively, and it is noted that the final resistance values are in the order $R_3''<R_2''<R_1''$ at the sensor operating temperature. The measured resistance values before and after exposure to H_2S for the three sensors are compared in Table III. The sensitivity defined as $S_n=R_n'/R_n''$, where $n=1$, 2 and 3 correspond to the three sensors SnO_2, SnO_2-CuO, and the SnO_2-CuO-dot, respectively, and their sensitivity is found to increase in the order $S_3>S_2>S_1$.

D. Starting resistance of the sensors in air

The observed increase in the starting resistance values ($R_3'>R_2'>R_1'$) of the three sensors can be explained as follows. The initial heat treatment of the as-deposited SnO_2-Cu bilayer sensors at 300 °C in air leads to the formation of a heterojunction at the $CuO–SnO_2$ interface.[18] The formation of the depletion region due to *p*-type CuO and *n*-type SnO_2 tends to reduce the effective thickness of the underlying SnO_2 layer through where the charge carriers can flow. Moreover diffusion of some amount of copper into SnO_2, and the formation of electronic barriers at the $CuO–SnO_2$ intergranular region in the bulk of the film cannot be precluded. Copper is known to diffuse extensively and can draw oxygen from SnO_2 to create intergranular ($CuO–SnO_2$) barriers. The combined effect of the depletion layer at the interface, and the interdiffusion of copper are therefore expected to yield a high value of the starting resistance for the SnO_2-CuO sensor (R_2'). A measured value of $R_2'=2196\ k\Omega$ and $R_3'=1596\ k\Omega$, and $R_2'>R_1'$ clearly support the expected behavior. The measured value of $R_2'=2196\ k\Omega$ could have been much higher, but for the expected contribution arising due to the removal of oxygen from the SnO_2 bulk, during the interdiffusion of Cu into SnO_2 and the transformation of Cu to CuO. In the SnO_2-CuO-dot structure [Fig. 5(d)] besides the depletion region and the interdiffusion of Cu into SnO_2, oxygen adsorbs on the uncovered SnO_2 surface between the CuO dots and captures electrons from the conduction band to remain as O_2^- and O^- ions until desorbed at a high temperature, or in the presence of a reducing gas. The oxygen adsorption in-

TABLE III. Variation in the measured resistance values of sensors.

Sensor type	Resistance of as-deposited (film/bilayers) (kΩ)	Starting resistance at the operating temperature (kΩ)	Resistance after exposure to H_2S (kΩ)	Sensitivity $S_n=R_n'/R_n''$
SnO_2	$R_1=3172$	$R_1'=1596$	$R_1''=141.8$	11.25
SnO_2-CuO	$R_2=4392$	$R_2'=2196$	$R_2''=12.92$	170
SnO_2-CuO-dot	$R_3=7356$	$R_3'=5550$	$R_3''=0.756$	7341
Relationship	$R_3>R_2>R_1$	$R_3'>R_2'>R_1'$	$R_3''<R_2''<R_1''$	

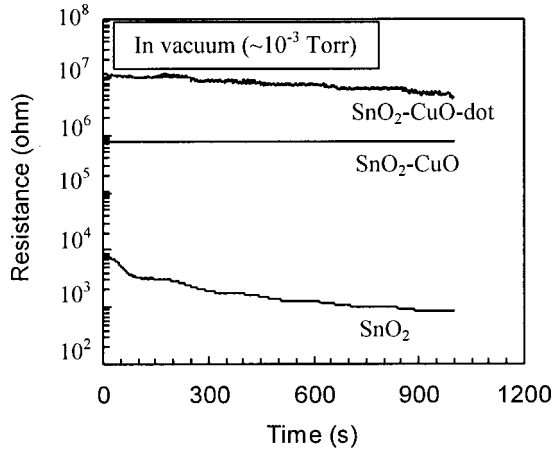

FIG. 6. Variation of starting resistance of the three sensors with time under vacuum.

creases the extent of depletion region between the CuO dots as shown in Fig. 5(d). Thereby the measured starting resistance (R_3') of the SnO_2-CuO-dot sensor is expected to increase further. The measured value of $R_3'=5550\ k\Omega$ is found to be over and above the value of R_2' obtained previously without the contribution from adsorbed oxygen, and clearly supports the observed trend $R_3'>R_2'>R_1'$.

1. Role of adsorbed oxygen

The role of adsorbed oxygen is examined by measuring the variation in sensor resistance at the operating temperatures under increasing vacuum, and the results are shown in Fig. 6. SnO_2, SnO_2-CuO, and SnO_2-CuO-dot sensors exhibited a decrease in their resistance values by 88%, 1.5%, and 61%, respectively, within 15 min in vacuum ($\sim 10^{-3}$ Torr). The observed decrease in the resistance of the three sensing elements (Fig. 6) was in accordance with the free SnO_2 surface area available in each of the sensor configurations.

In the case of pure SnO_2 film the resistance ($R_1=R_{SnO_2}$) is primarily determined by the amount of oxygen adsorbed on its surface, and the absence of adsorbed oxygen on the surface of SnO_2-CuO sensor support the insignificant change in resistance value (R_2). However, a change in the resistance value by 61% in the case of SnO_2-CuO-dot sensor clearly indicates the dominant role played by the adsorbed oxygen besides the depletion layer at the SnO_2-CuO interface and the grain boundaries due to Cu diffusion into SnO_2. Earlier investigations have reported that the space charge layer at the interface is dependent on many factors including; surface coverage of oxygen adsorbates,[19] the intrinsic electron concentration in the bulk,[19] the grain size,[20] the presence of foreign[21] metal oxides in SnO_2, and the oxidation state of the loaded metal on the SnO_2 surface.[22]

Thus equivalent resistance values R_2 and R_3 are not a simple parallel combination of R_{SnO_2} and R_{CuO}, but are influenced by the distribution of CuO on the SnO_2 surface. In the case of SnO_2-CuO-dot sensor, the starting resistance is therefore the summation of the contribution from the formation of depletion region at the interface, due to diffused copper in the bulk of SnO_2 and the adsorbed oxygen at the uncovered SnO_2 surface.

E. Resistance in the presence of H_2S gas

1. SnO_2-CuO sensor

A processing temperature of 300 °C for the sensor element fabrication ensured the oxidation of Cu to CuO, which is the most stable oxidation state at low temperatures.[17] In the presence of H_2S and air CuO converts to CuS. Formation of Cu_2S in miniscule quantity cannot be ruled out due to the slow reduction of CuS by hydrogen (from H_2S), and other compounds such $CuSO_4$ and Cu_2SO_4 are not expected as they demand either very high temperatures (~1000 °C), or the presence of Cu_2O initially for the reaction.[17]

The chemical reaction at the SnO_2-CuO surface with H_2S is given by

$$CuO+H_2S\rightarrow CuS+H_2O. \quad (2)$$

The final sensor resistance at its operating temperature (150 °C) in H_2S is influenced by a number of factors. First, CuO converts to CuS, which is reported to be more metallic[22] than CuO. This tends to make the CuO region less *p* type and allows the depletion region at the interface to extend more into the *p*-type CuO and less into the *n*-type SnO_2. Second, at 150 °C the intergrain $CuO-SnO_2$ boundaries in the bulk of the SnO_2 film may be influenced by the penetrating H_2S through the grain boundaries. The penetration depth of H_2S deep into SnO_2 may be speculative, but thin polycrystalline SnO_2 layers that are porous can be expected to exhibit an enhanced effect. As a consequence the measured resistance of the sensor decreases and yields $R_2''<R_2'$ in the presence of H_2S, and leads to an increase in the sensitivity ($S_2=R_2'/R_2''=170$) for the SnO_2-CuO sensor in comparison to SnO_2 sensor ($S_1=R_1'/R_1''=11$). It is interesting to note that the increase in sensitivity is not only due to the increase in the starting resistance value ($R_2'>R_1'$), but also due to the lowering of the final resistance ($R_2''<R_1''$, values given in Table III).

It may be noted that the decrease in R_2'' with respect to R_1'' is limited and thereby only a small increase in the sensitivity from 11 to 170 is observed. The incoming H_2S converts the top CuO layer into CuS and increases the effective thickness of the SnO_2 layer through which charge carriers can traverse. Thereafter the H_2S is unable to penetrate deep enough to reduce the barriers with the interdiffused Cu in the bulk and is therefore almost ineffective despite increasing the sensor temperature.

After the removal of H_2S gas, CuS converts back to CuO in the presence of oxygen at the operating temperature (150 °C) by the following reaction:

$$CuS+3/2O_2\rightarrow CuO+SO_2, \quad (3)$$

where CuO formation regains the original state of depletion region at the SnO_2-CuO interface. Consequently the resistance of the sensor begins to increase to regain its initial high resistance value (R_2'). However the recovery is found to be relatively slow during phase I and fast during phase II as

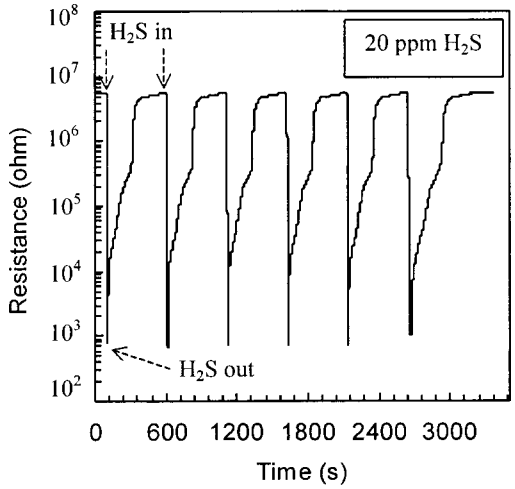

FIG. 7. Repetitive response and recovery characteristics of SnO_2-CuO-dot sensor under static condition.

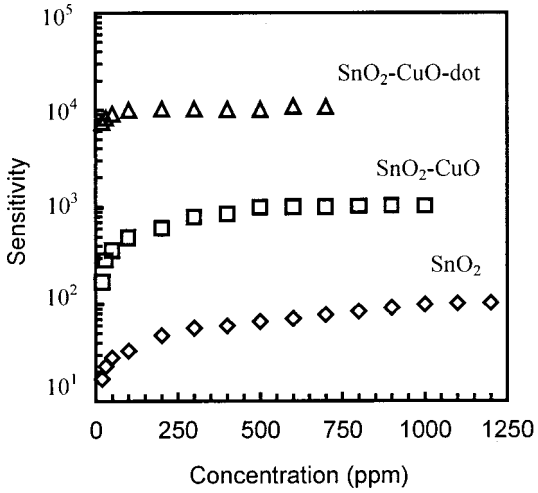

FIG. 8. Gas concentration characteristics of (a) SnO_2, (b) SnO_2-CuO, and (c) SnO_2-CuO-dot sensors.

contrary to SnO_2 sensor (Fig. 4) under the static condition. This is possible due to the slow rate of reaction [Eq. (3)] because under the static conditions the presence of SO_2 leads to the competing effect preventing complete reconversion of CuS to CuO quickly at 150 °C. The modulation of depletion region due to the formation of more *p*-type CuO is responsible for the fast rise as compared to SnO_2 sensor in phase II.

2. SnO_2-CuO-dot sensor

In the case of SnO_2-CuO-dot sensor the CuO and the uncovered SnO_2 surfaces are exposed to H_2S simultaneously. The conversion of CuO to metallic CuS shifts the extent of depletion region towards the *p*-type CuO and increases the effective thickness of SnO_2 layer. Moreover, Cu present in the form of CuO is known to initiate hydrogen spillover because it chemisorbs hydrogen rather weakly,[25] and the hydrogen atoms on its surface are highly mobile.[26] The hydrogen after spillover quickly interacts with the adsorbed oxygen and removes it from the uncovered SnO_2 surface between the dispersed CuO islands. This removal of oxygen leaves behind the excess free electrons that are available for conduction. Furthermore, the presence of grain boundaries in the polycrystalline SnO_2 allow the penetration of H_2S deep inside the bulk and reduces the barrier height at intergranular $CuO-SnO_2$ interface. This leads to a rapid decrease in the measured final resistance value ($R_3''=0.756\ \mathrm{k}\Omega$). It is nearly three orders of magnitude lower than the starting resistance value ($R_3'=5550\ \mathrm{k}\Omega$) and yields a high sensitivity ($S_3=R_3'/R_3''=7.3\times10^3$) with a fast response time of 14 s (Fig. 3).

After removal of H_2S the recovery under a static condition (Fig. 4) was initially slow in phase I, and was followed by a sudden rise in phase II. The adsorption of oxygen at the uncovered SnO_2 surface (phase I) leads to the slow rise in

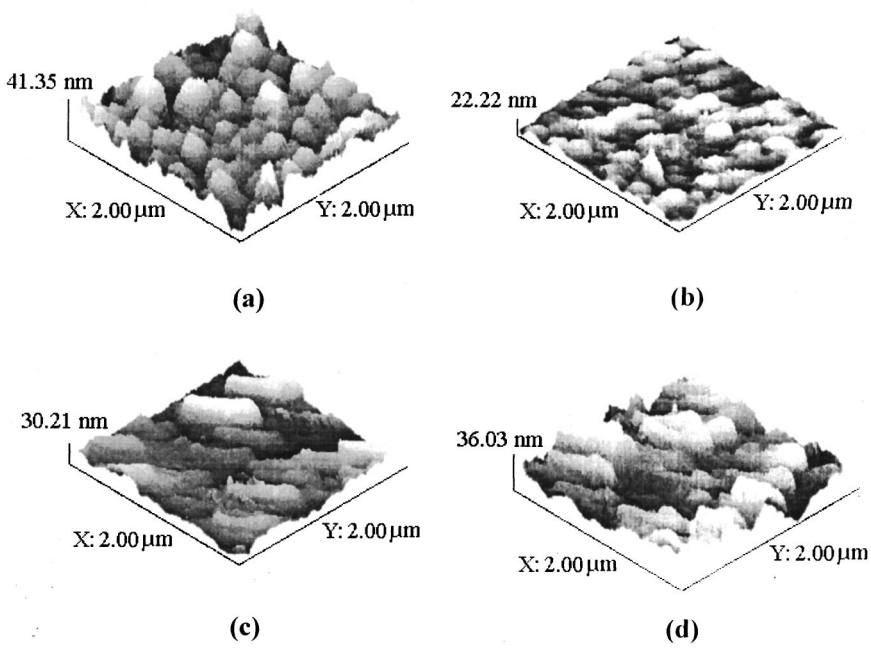

FIG. 9. AFM profiles of as-deposited surfaces of (a) SnO_2-CuO and (b) SnO_2-CuO-dot sensors, (c) sensor surface after heat treatment at 300 °C in air, and (d) sensor surface after exposure to 20 ppm H_2S.

the resistance initially. The rise in resistance in phase II seems to be governed at two different rates [Fig. 4(c)]. The barrier heights at the intergranular boundaries begin to increase with the gradual penetration of oxygen into the bulk. By the time modifications in the bulk are nearing completion, the top CuS islands are reconverting completely to CuO and thus give rise to a sudden jump in the recovery characteristics under static condition [Fig. 4(c)]. The recovery of the sensor is much faster under the dynamic condition because the availability of the oxygen is more on the sensor surface.

Figure 7 represents the response in a repetitive run involving H_2S gas sensing and the recovery alternately for the SnO_2-CuO-dot sensor. The sensor exhibited good reproducibility and a fast response for about five runs successively, but for the sixth run the recovery was slow, and the sensitivity decreased slightly. However, heating in air for 90 min at 150 °C the sensor regained its original starting resistance and sensitivity, and could be used reproducibly. The onset of degradation of the sensor seems to occur due to the incomplete reverse transformation of CuS to CuO at 150 °C, and the ultimate poisoning of the sensor can be attributed to the higher residence time of the adsorbate (sulphur). Figure 8 shows the variation in sensitivity with increasing concentration of H_2S gas in the range 20 to 1200 ppm. The sensitivity of the SnO_2-CuO-dot increases from 7.3×10^3 to $\sim10^4$ and is found to saturate at 200 ppm, whereas the SnO_2 sensor saturated relatively at a higher concentration (1200 ppm) with a sensitivity of 117. The high sensitivity of the SnO_2-CuO-dot sensor at 20 ppm H_2S appears to be promising and useful for detecting a much lower concentration of H_2S gas.

IV. ATOMIC FORCE MICROSCOPY ANALYSIS

Figures 9(a) and 9(b) show the atomic force microscopy (AFM) images of the as-deposited surfaces of the SnO_2-CuO and SnO_2-CuO-dot sensors. The as-deposited polycrystalline SnO_2-CuO bilayer [Fig. 9(a)] exhibited a dense surface that was rough consisting of round shaped grains. In comparison the roughness was less [Fig. 9(b)] in the case of dotted CuO islands on SnO_2 surface, and the grain size was small. Figure 9(c) represents the typical image obtained on all three sensor surfaces after the initial heat treatment in air at 300 °C, and a significant change in the surface morphology is observed. The spherical grains shown in Figs. 9(a) and 9(b) are transformed into smooth elongated structures as shown in Fig. 9(c) with channels, and step formations leading to increase in surface roughness. Especially in the case of the SnO_2-CuO-dot sensor the elongated grains were disconnected, and seemed to expose the underlying SnO_2 surface between the grains. Figure 9(d) represents the image obtained from the sensor surfaces exposed to 20 ppm H_2S gas. The surface of elongated grains appears to become rough, and there is some kind of an overgrowth on the surface after H_2S exposure.

V. CONCLUSIONS

The enhanced sensitivity and response speed of CuO dotted SnO_2 sensors in comparison to the other two sensors SnO_2, SnO_2-CuO reveals the importance of the Cu catalyst layer distribution on the SnO_2 film. The increasing sensitivity for the SnO_2, SnO_2-CuO, and SnO_2-CuO-dot sensors is found to depend primarily on the modulation of the depletion region at the SnO_2-CuO interface. The modulation of the electronic barriers due to the interaction of H_2S gas with CuO via grain boundaries, and the spillover effect of H_2 in the case of SnO_2-CuO-dot sensor are found to enhance the sensitivity significantly. A systematic variation of the starting and final resistance of the sensors before and after exposure to the H_2S is found to depend strongly on changes occurring at the surface and in the bulk. Ultrathin CuO film in the form of dotted islands on SnO_2 film is found to exhibit a high sensitivity ($S=7.3\times10^3$) at a low operating temperature (150 °C), and a fast response (14 s) in comparison to earlier reported results on H_2S gas sensors. The enhanced sensitivity and response with ultrathin CuO dotted islands clearly point to the vital role of the spillover mechanism besides the Fermi level type of interaction. Hydrogen from the dissociated H_2S gas molecule is seen easily to ''spillover'' onto the SnO_2 and increase the sensitivity considerably. The formation of elongated grains providing a large surface area seems to enhance the sensitivity in the SnO_2-CuO-dot sensor.

ACKNOWLEDGMENTS

One of the authors (A.C.) thanks the Council of Scientific and Industrial Research (CSIR), India, for a research fellowship, P.S. thanks the Royal Institute of Technology (KTH), Stockholm for a visiting fellowship, and all of the authors thank Professor Abhai Mansingh for fruitful discussions.

[1] K. Ihokura and J. Watson, in *The Stannic Oxide Gas Sensor, Principles and Applications* (CRC, Boca Raton, FL, 1994).
[2] M. N. Rumyantseva, M. Labeau, J. P. Senateur, G. Delaboulglise, M. N. Boulova, and A. M. Gaskov, Mater. Sci. Eng., B **41**, 228 (1996).
[3] J. Tamaki, K. Shimanoe, Y. Yamada, Y. Yamamoto, N. Miura, and N. Yamazoe, Sens. Actuators B **49**, 121 (1998).
[4] T. Maekawa, J. Tamaki, N. Miura, and N. Yamazoe, Chem. Lett. , 575 (1991).
[5] S. Kanefusa, M. Nitta, and M. Haradome, IEEE Trans. Electron Devices **35**, 65 (1988).
[6] V. Lantto, P. Romppainen, T. S. Rantala, and S. Leppavuori, Sens. Actuators B **4**, 451 (1991).
[7] L. Jianping, W. Yue, G. Xiaoguang, M. Qing, W. Li, and H. Jinghong, Sens. Actuators B **65**, 111 (2000).
[8] R. B. Vasiliev, M. N. Rumyantseva, S. E. Podguzova, A. S. Ryzhikov, L. I. Ryabova, and A. M. Gaskov, Mater. Sci. Eng., B **57**, 241 (1999).
[9] C. H. Liu, L. Zhang, and Y. J. He, Thin Solid Films **304**, 13 (1997).
[10] M. S. Tong, G. R. Dai, and D. S. Gao, Vacuum **59**, 877 (2000).
[11] T. Maekawa, J. Tamaki, N. Miura, and N. Yamazoe, J. Mater. Chem. **4**, 1259 (1994).
[12] D. J. Yoo, J. Tamaki, S. J. Park, N. Miura, and N. Yamazoe, Jpn. J. Appl. Phys., Part 1 **34**, L455 (1995).
[13] M. Egashira, T. Matsumato, Y. Shimizu, and H. Iwanaga, Sens. Actuators **14**, 205 (1988).
[14] J. Tamaki, T. Maekawa, N. Miura, and N. Yamazoe, Sens. Actuators B **9**, 197 (1992).
[15] S. Gadkari, V. Katti, A. Debnath, K. Muthe, S. Gupta, and V. Sahni. Proceeding of NSPTS-8, IGCAR, Kalpakkam, India C 2.1 (2001).
[16] S. R. Morrison, Sens. Actuators **12**, 425 (1987).

[17] W. M. Latimer and J. H. Hildebrand, in *Reference Book of Inorganic Chemistry*, 3rd ed. (Macmillan, New York, 1951).
[18] S. Manorama, G. Saraladevi, and V. J. Rao, Appl. Phys. Lett. **64**, 3163 (1994).
[19] K. Ihokura, New Mater. Proc. **1**, 43 (1981).
[20] H. Ogawa, M. Nishikawa, and A. Abe, J. Appl. Phys. **53**, 4448 (1982).
[21] C. Xu, J. Tamaki, N. Miura, and N. Yamazoe, Sens. Actuators B **3**, 147 (1991).
[22] Y. Takao, Y. Iwanaga, Y. Shimizu, and M. Egashira, Sens. Actuators B **10**, 229 (1993).
[23] M. Gaidi, B. Chevenier, and M. Labeau, Sens. Actuators B **62**, 43 (2000).
[24] J. Mizsei and V. Lantto, Sens. Actuators B **4**, 163 (1991).
[25] G. C. Bond, in *Proceedings of the International Symposium, Lyon-Villeurbanne*, edited by G. M. Pajonk, S. J. Teichner, and J. E. Germain (Elsevier, New York, 1983).
[26] R. Kramer and M. Andre, J. Catal. **58**, 287 (1979).